

Mechanical and Corrosion Properties of Magnesium–Hydroxyapatite (Mg–HA) Composite Thin Films

K. Mensah-Darkwa¹⁾, R.K. Gupta^{2)*}, D. Kumar¹⁾

1) Engineering Research Center of Revolutionizing Metallic Biomaterials, Department of Mechanical Engineering, North Carolina A & T State University, 1601 East Market Street, Greensboro, NC 27411, USA

2) Department of Chemistry, Pittsburg State University, 1701 S. Broadway, Pittsburg, KS 66762, USA

[Manuscript received November 15, 2012, in revised form January 4, 2013, Available online 18 April 2013]

Magnesium (Mg)–hydroxyapatite ($\text{Ca}_{10}(\text{PO}_4)_6(\text{OH})_2$, abbreviated as HA) composite films have been grown on Mg plates using a pulsed laser deposition technique. Mechanical property measurements and analysis have indicated that hardness and Young's modulus of $n\text{Mg}-(100-n)\text{HA}$ composite coatings increase with Mg content in the coatings and reach a maximum at a 70Mg–30HA composition. n and $100-n$ in the $n\text{Mg}-(100-n)\text{HA}$ represent the relative number of laser pulses impinging on Mg and HA targets, respectively. Direct current potentiodynamic polarization studies have shown that the corrosion of Mg plate (control) decreases with an increase in the HA ratio in the composite films. For example, the corrosion current density of Mg plate reduces by ~ 350 times after coating the Mg plate with 10Mg–90HA composite film. The reduction in corrosion current density of Mg plates was also accompanied by a positive shift in the corrosion potential ($\sim 6\%$) due to this coating. The mechanism behind the reduction in corrosion behavior of Mg plates due to $n\text{Mg}-(100-n)\text{HA}$ composite coatings has been understood by electrochemical impedance spectroscopy.

KEY WORDS: Magnesium; Hydroxyapatite; Scanning electron microscopy; Pulsed laser deposition; Corrosion; Impedance spectroscopy

1. Introduction

Magnesium and its alloys are of great interest for biomedical applications because of their promising biocompatibility and self-degradability in the living beings^[1]. Apart from the biocompatibility, they possess other promising advantages such as low density, high specific strength, castability and appropriate hardness^[2]. However, a high corrosion rate of Mg bringing about a swift release of undesirable corrosion products is still preventing practitioners from its application and deployment in living beings as implants where a deliberate dissolution of Mg is needed in order for it to be biodegradable^[3]. A slow dissolution of Mg implants could be very advantageous for bone cell attachment and tissue growth around the Mg implants^[4]. Therefore, in order to use Mg as effective implants, the corrosion rate of Mg needs to be slowed down. Hence, laying a protective coating on Mg consisting of bioactive materials which are non-toxic as well as biocompatible would enhance its applicability as bioresorbable bone implants^[5].

Different methods such as alloying, surface modification, and coatings have been used to modify the corrosion rate of Mg^[3,6–9]. Surface modification/coating is an extensively studied method used to improve the performance of biomaterials in physiological environment^[10–13]. It offers the prospects of modifying the surface properties of an implant tailored to a specific application without compromising the bulk properties of an implant^[14,15]. Among the various surface modification/coating materials to slow down the corrosion rate and improve mechanical and biological properties of Mg and its alloys^[16–21], HA based coating is very unique because of its similar chemical and crystallographic structure to bone^[22,23]. HA also promotes new bone tissue formation and accelerates the bone growth^[16]. It is highly corrosion resistive, non-toxic, and biocompatible^[17]. The distinctiveness of our method is its ability to precisely adjust the mechanical (Young's modulus, Hardness) and corrosion properties by varying the composition of Mg–HA coating simply by changing the relative number of laser pulses impinging on Mg and HA targets. Mg–HA bulk composites with variable mechanical and corrosion properties have been prepared in bulk form using standard powder metallurgy method which is time-consuming putting a severe limitation in producing bulk materials with a larger variation in composition and stoichiometry^[18]. This limitation for bulk synthesis might also prevent reaching an optimum composition of the composite as opposed to the pulsed laser deposition (PLD) method where composition optimization is based on combinatorial

* Corresponding author. Ph.D.; Tel.: +1 6202354763; Fax: +1 6202354003; E-mail address: ramguptamsu@gmail.com (R.K. Gupta).
1005-0302/\$ – see front matter Copyright © 2013, The editorial office of Journal of Materials Science & Technology. Published by Elsevier Limited. All rights reserved.
<http://dx.doi.org/10.1016/j.jmst.2013.04.019>

approach. It should be however noted that there are some recent work reporting the fabrication of Mg doped HA films on non-absorbable implant surfaces^[24]. In this work^[24], Mroz *et al.* showed that doping HA with low concentration of Mg results in improvement in osteoblast adhesion as compared to pure HA films. The problem with their method is the difficulty in the fabrication of dense Mg–HA targets with exact composition due to difference in melting points as well as vapor pressures of Mg and HA.

In the present paper, we report a significant improvement in the mechanical and corrosion properties of Mg plates, the two key properties of a biodegradable implant, by means of depositing $n\text{Mg}-(100-n)\text{HA}$ (hereafter Mg–HA) composite films on Mg plates. The composite films having different amount of Mg and HA were deposited on Mg plates as substrates using a multi-target PLD system at room temperature. The detailed structural, mechanical, and corrosion properties of the Mg–HA coated Mg plates and uncoated Mg plate (control) have been studied.

2. Experimental

Mg target for the PLD was prepared by cutting high purity (99.7%) Mg rod (Goodfellow, Germany). HA target was prepared using cold pressing of HA powder (Sigma–Aldrich, USA) at $6 \times 10^6 \text{ N/m}^2$ load followed by sintering at 800°C for 15 h. The films having different compositions were deposited using KrF excimer laser (Lambda Physik COMPex, $\lambda = 248 \text{ nm}$ and pulsed duration of 20 ns). The laser was operated at a pulse rate of 10 Hz with energy density of 2 J/cm^2 . $n\text{Mg}-(100-n)\text{HA}$ composite films with different n were deposited on Mg plates (control) at room temperature in vacuum in excess to $5 \times 10^{-6} \text{ Torr}$ ($0.667 \times 10^{-3} \text{ Pa}$). The exact weight ratio of the Mg–HA composite films is given in Table 1 along with their pulse ratio. Before deposition of the films, the Mg plates were progressively polished with SiC paper upto grade #1200 and followed by degreasing in acetone. The thickness of each film was measured by using a cross section scanning electron microscope (SEM, SU8000, Hitachi).

The microstructures of uncoated Mg plate and Mg plates coated with various composition of Mg–HA were recorded before and after corrosion process by scanning electron microscopy (SEM). The structural characterizations were performed by X-ray diffraction (XRD) technique. The XRD spectra of the films were recorded under a Bruker AXS (D8 Discover) X-ray diffractometer using the 2θ – θ scan with $\text{CuK}\alpha$ ($\lambda = 0.15405 \text{ nm}$) radiation. Materials composition and homogeneities of Mg and HA in the composite films were studied with an energy dispersive spectrometer (EDS, Quantax 200, Bruker). The mechanical properties of the uncoated Mg plate and Mg plates coated with

various Mg–HA compositions were studied using a nano-indenter (CSEM Instruments) where indentations were made using a Berkovich diamond indenter. The strain rate and dwell time at maximum load was 0.05 s^{-1} and 10 s, respectively.

Direct current potentiodynamic polarization measurements were performed in phosphate buffered saline (PBS) solution (137 mmol/L-NaCl , 2.7 mmol/L-KCl , $10 \text{ mmol/L-Na}_2\text{H-PO}_4 \cdot 2\text{H}_2\text{O}$, $2.0 \text{ mmol/L-KH}_2\text{PO}_4$) using Gamry Potentiostat/Galvanostat/ZRA (R600, Gamry Instruments) with a standard three-electrode configuration. Ag/AgCl (saturated KCl) and platinum wire were used as the reference and counter electrodes, respectively. Uncoated Mg plate and Mg plates coated with Mg–HA composite films were used as the working electrodes. Before recording the potentiodynamic polarization curves, uncoated Mg plate and Mg plates coated with the Mg–HA composite films were soaked in the PBS solution to get the steady state reaction condition. Under the steady state corrosion condition, the open-circuit potential becomes constant with time. The volume of the PBS solution was taken as 50 mL. Corrosion potential and current density were calculated using the Echem Anlyst software (Gamry Instruments). The electrochemical impedance spectroscopy (EIS) study was performed in the frequency range of $1-10^6 \text{ Hz}$ under 10 mV amplitude of the perturbation signal. The EIS measurements were performed at the open-circuit potential of the samples and recorded with Gamry Potentiostat/Galvanostat/ZRA (R600, Gamry Instruments). The impedance data were analyzed using the Echem Anlyst software.

3. Results and Discussion

3.1. Structural characterizations

3.1.1. Scanning electron microscopic studies. The SEM images of the uncoated Mg plates (control sample) and Mg plates coated with various Mg–HA composite films are shown in Figs. 1 and 2. As seen in these images, the films having higher amount of Mg show the presence of larger number of droplets in comparison to the films having larger amount of HA. Clearly, the number density of these droplets decreases with an increase in the HA content in the composite films. The presence of a higher droplet density in the Mg–HA composite films with respect to that in pure HA films is attributed to the ablation characteristics of a metal target. A metal target possesses relatively high thermal conductivity and high optical reflectivity. Both of these parameters lead to high fluence requirement which results in splashing (ejection of clusters) from metal target^[25]. An implant surface coated with a biocompatible materials having the droplet/particulate features has been found to increase cell growth, proliferation, and anchorage with surrounding tissues^[26]. The EDS results have revealed that there is a slight increase in the Ca/P ratio in the pure HA films compared to commercially available bulk hydroxyapatite powder (Ca/P = 1.67). This could be due to the loss of phosphorous from the film during the deposition process as the vapor pressure of phosphorous is significantly higher ($\sim 10 \text{ Pa}$ at room temperature) than that of calcium (almost zero at room temperature)^[27,28]. Fig. 3 shows elemental mapping images of Mg plates coated with 50Mg–50HA composite film as a representative. It can be seen from Fig. 3(a) that the droplets observed in the SEM images were rich in Mg. The elemental mappings also suggest a very uniform distribution of elements (e.g. Mg, Ca, P, O) in the composite films. The film thickness of the composite films was measured using cross

Table 1 Composition of the various composite films along with their pulse ratio

Sample	Pulse ratio	Weight ratio
	(Mg/HA)	(Mg/HA)
100Mg	100/0	100/0
70Mg–30HA	70/30	42.9/57.1
50Mg–50HA	50/50	24.3/75.7
10Mg–90HA	10/90	3.5/96.5
100HA	0/100	0/100

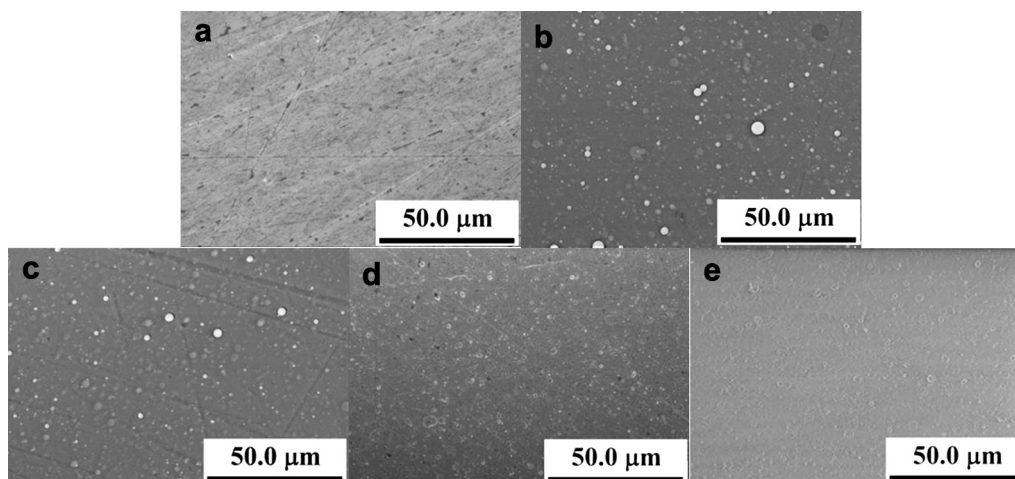


Fig. 1 SEM images of (a) uncoated Mg plate and Mg plates coated with (b) 70Mg–30HA, (c) 50Mg–50HA, (d) 10Mg–90HA, and (e) 100HA films.

section SEM images as shown in Fig. 4. The thickness of films having composition of 70Mg–30HA, 50Mg–50HA, 10Mg–90HA, and 100HA was observed to be 4.12, 4.30, 4.48, and 6.12 μm , respectively.

3.1.2. X-ray diffraction studies. The XRD patterns of uncoated Mg plates and Mg plates coated with the Mg–HA composite films are shown in Fig. 5(a). For the uncoated Mg plate (control), all the peaks detected could be labeled corresponding to a hexagonal phase of polycrystalline bulk Mg (JCPDS file 035-0821) with a lattice parameters of a and c equal to 0.32094 nm and 0.52112 nm, respectively. The full width at half maximum (FWHM) of (002) peak from Mg plates seems to have broadened upon coating with the composite films. This broadening may be due to the presence of nanocrystalline phase of Mg in the composite films since both HA and Mg were grown at room temperature. Since Mg–HA composite films were grown at room temperature, HA is present in amorphous phase. It is not uncommon to miss XRD peaks from amorphous films, especially when the peaks from the substrate materials are strong. However, the logarithmic plot of the composite films does show

signal of HA in the composite. Fig. 5(b) shows a logarithmic plot of 70Mg–30HA as a representative plot. The (120), (300), (301), and (113) peaks corresponding to HA phase are now noticeably present. Since the surface energy of metal is relatively small, Mg grows with a polycrystalline structure even at room temperature and hence strong peaks due to Mg are present in XRD patterns. Dinda *et al.*^[26] also witnessed the amorphous nature of HA films grown using PLD at room temperature. Witte *et al.*^[18] and Gu *et al.*^[16] also observed a similar overlapping and broadening of Mg peaks around (002) position in the X-ray diffraction patterns of Mg in Mg–HA bulk composites. Recently, Mroz *et al.*^[24] reported that changes in the concentration of HA component in Mg–HA composites alter the X-ray diffraction patterns from crystalline to amorphous phase.

3.2. Mechanical properties

The mechanical properties of the uncoated Mg plate and Mg plates coated with Mg–HA composite films were studied by using a Berkovich nanoindenter which is considered as one of

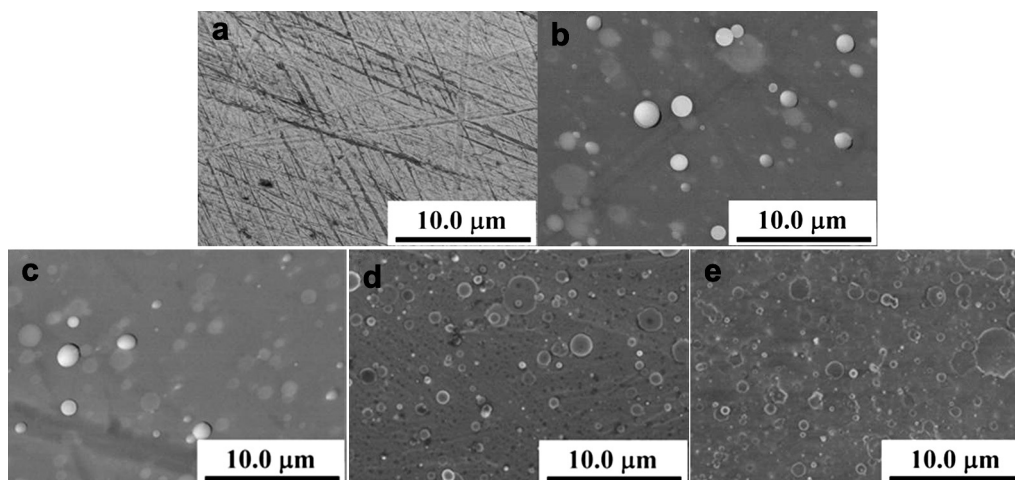


Fig. 2 Higher magnification SEM images of (a) uncoated Mg plate and Mg plates coated with (b) 70Mg–30HA, (c) 50Mg–50HA, (d) 10Mg–90HA, and (e) 100HA films.

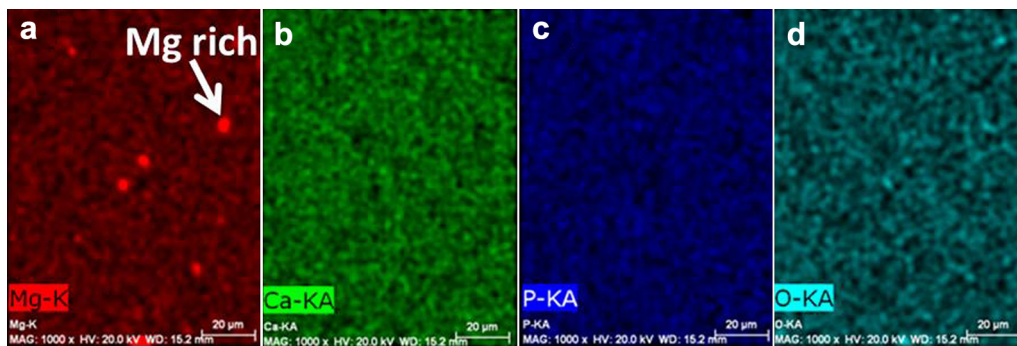


Fig. 3 Elemental mapping of 50Mg–50HA composite film coated on Mg plate.

the very suitable and accurate methods to determine the mechanical properties of thin films and composites^[29]. The nano-indentation results suggest that Mg–HA composite coatings possessed superior mechanical properties with respect to Mg plates (control) in terms of hardness as well as elastic modulus values. The values and the behavior of the hardness and elastic modulus of the Mg–HA composite films as well as bulk Mg are in good agreement with the findings in the open literature^[11,26,30–33]. As shown in Fig. 6, the hardness value increases consistently with increase in Mg content (0–70%) in the film from 1.5 to 2.7 GPa. On the other hand, elastic modulus values varied from 47 to 62 GPa with increasing Mg content from 0 to 70%. Chamos *et al.*^[33] studied the mechanical properties of bulk Mg and observed a hardness of 1.1 GPa and elastic modulus of ~55 GPa. The observed values of hardness (1.0 GPa) and elastic modulus (38 GPa) in this work are in good agreement with the values reported for bulk Mg^[33]. However, the elastic modulus values measured in this work show some difference to values

reported in literature. This difference may be due to the surface effects such as surface roughness and surface oxidation of Mg^[33]. Even though, there are no data reported on the mechanical properties for Mg–HA composite films *per se*, there are some reports on mechanical properties of pure HA films. According to these reports, hardness value ranges from 0.5 to 2.0 GPa and elastic modulus from 74 to 82 GPa for pure HA films^[11,30,32,34].

3.3. Potentiodynamic polarization study

The polarization measurements were carried out in the applied potential range of ± 300 mV around open-circuit potential. The scan rate employed was 5 mV/s. The pH of the solution before and after corrosion was measured and found to be constant (~ 7.4). Fig. 7 shows the polarization curves for the uncoated Mg plate and Mg plates coated with the Mg–HA composite films. The corrosion potential (E_{corr}) and corrosion current

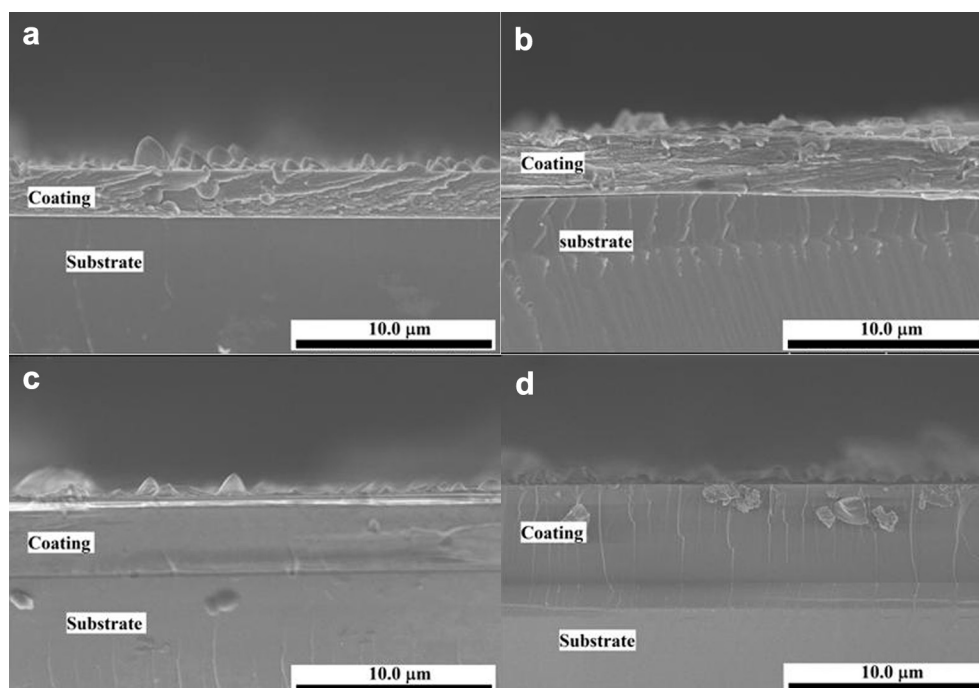


Fig. 4 Cross section SEM images of Mg plates coated with (a) 70Mg–30HA, (b) 50Mg–50HA, (c) 10Mg–90HA, and (d) 100HA films.

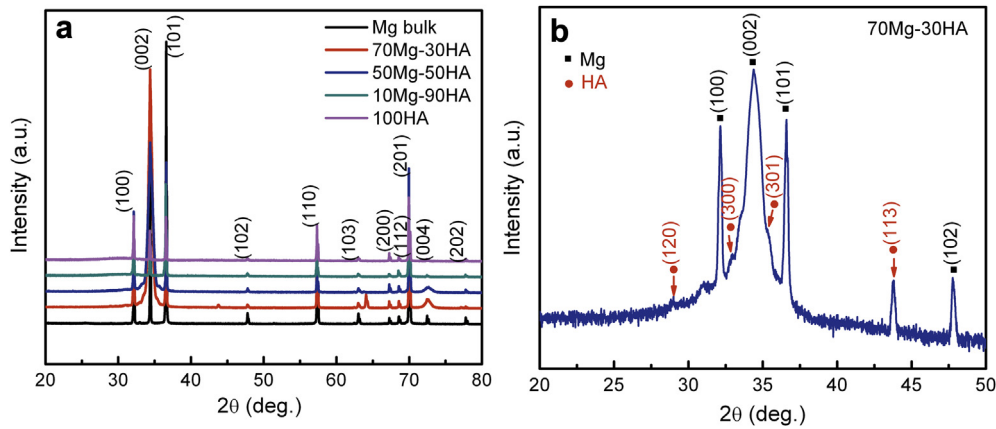


Fig. 5 (a) XRD patterns of uncoated Mg plate (control) and Mg plates coated with Mg–HA composite films having various compositions, and (b) logarithmic XRD patterns of 70Mg–30HA composite films coated on magnesium substrate.

density (I_{corr}) were estimated by using the Stern–Geary equation^[35]:

$$I_{\text{corr}} = \frac{1}{2.303R_p} \left(\frac{\beta_a \times \beta_c}{\beta_a + \beta_c} \right) \quad (1)$$

where R_p is the corrosion resistance in $\Omega \text{ cm}^2$, β_a is the anodic Tafel slope in Volt/decade, and β_c is the cathodic Tafel slope in Volt/decade. The corrosion potential was estimated to be -1.59 V for uncoated Mg plate while the corrosion potential values were calculated to be -1.57 , -1.54 , -1.49 , and -1.49 V for Mg plates coated with 70Mg–30HA, 50Mg–50HA, 10Mg–90HA, and 100HA films, respectively. As seen in Fig. 7, the E_{corr} of the Mg plates coated with Mg–HA composite films shifts positively from -1.57 to -1.49 V as the HA content in the film increases from 30% to 100%. The increase in E_{corr} indicates that the coated Mg plate is more cathodic compared to uncoated Mg plate, i.e. the coated Mg plates will have less tendency to lose its electrons and thus will be more corrosion resistive compared to uncoated Mg plate. Wen et al.^[36] also found that E_{corr} of Mg alloy (AZ31) shifted positively from -1.60 to -1.42 V after electro-deposition of HA on Mg alloy. On the other hand, I_{corr} of uncoated, 70Mg–30HA, 50Mg–50HA, 10Mg–90HA and 100HA composite film coated Mg plates were 1.21×10^{-5} , 1.38×10^{-6} , 2.52×10^{-7} , 3.27×10^{-8} , and

$4.68 \times 10^{-10} \text{ A/cm}^2$, respectively. Clearly, I_{corr} of the Mg–HA coated Mg plates decreases significantly as the HA content of the films increases. The positive shift in the corrosion potential and low corrosion current density for Mg–HA composite films coated Mg plates indicates the corrosion protective nature of these coating on Mg. As evident from the E_{corr} and I_{corr} for the coated Mg plates, the composite films having higher amount of HA is more corrosion protective in nature. The corrosion protective nature of the Mg–HA coatings was further analyzed on the basis of protection efficiency. The protection efficiency (PE) of the Mg–HA composite coatings on the Mg plates was estimated using the equation given below^[37]:

$$\text{PE}(\%) = \frac{i_{\text{corr}} - i'_{\text{corr}}}{i_{\text{corr}}} \times 100 \quad (2)$$

where, i_{corr} and i'_{corr} are the corrosion current density of the uncoated Mg plate and Mg plates coated with Mg–HA composite films, respectively. The protection efficiency of 70Mg–30HA, 50Mg–50HA, 10Mg–90HA and 100HA coated Mg plates were calculated to be 88.6%, 97.9%, 99.7%, and 99.9%, respectively. As observed, the corrosion protection

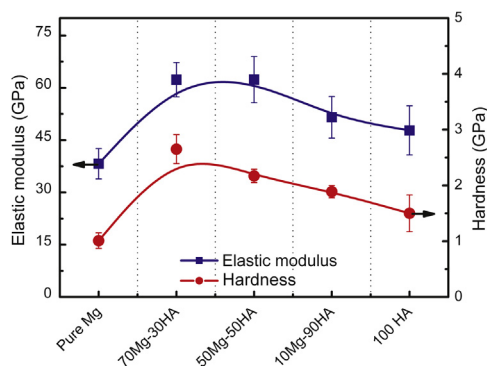


Fig. 6 Elastic modulus and hardness for uncoated Mg plate (control sample) and Mg plates coated with Mg–HA composite films having various compositions.

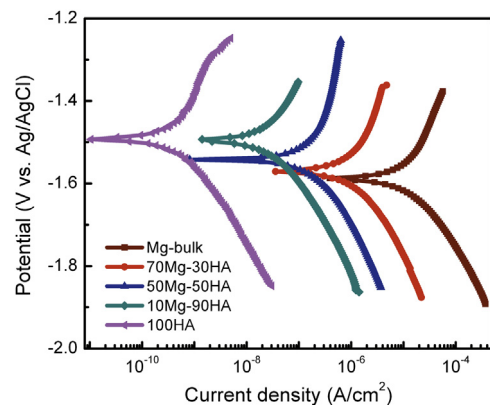


Fig. 7 Potentiodynamic polarization curves for Mg plate (control) and Mg plates coated with Mg–HA composite films having various compositions.

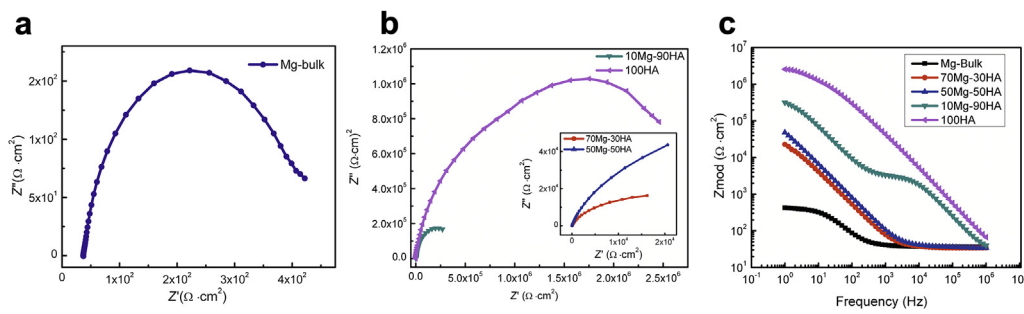


Fig. 8 Nyquist (a,b) and Bode (c) plots for uncoated Mg plate (control) and Mg plates coated with Mg–HA composite films having various compositions.

efficiency of the Mg–HA coatings increases with the increase of HA composition in composite films.

3.4. Electrochemical impedance spectroscopic analysis

The corrosion protective nature of the Mg–HA composite films on Mg plates was further analyzed by electrochemical impedance spectroscopy (EIS). In EIS, information about the corrosion protection efficiency of coatings is obtained by measuring the changes in impedance as a function of coating materials. Fig. 8 shows Nyquist and Bode plots of the uncoated Mg plate and Mg plates coated with Mg–HA composite films at an applied potential corresponding to the value of the open-circuit potential. The inset of Fig. 8(b) shows the Nyquist plots for 70Mg–30HA and 50Mg–50HA coated Mg plates. As seen in these figures, the arc for Mg–HA coated Mg plates shows a larger radius of curvature in comparison with that of the uncoated Mg plate. The larger radius of curvature of the Nyquist plots recorded for Mg plates coated with Mg–HA composite

films implies a higher impedance of the coatings. Fig. 8(c) shows the Bode plots for uncoated Mg plate and Mg plates coated with various Mg–HA composite films. As seen in the figure, impedance of the Mg–HA composite films on Mg plates is higher than uncoated Mg plate. The higher impedance of the composite coatings prevents the diffusion of the electrons and ions from the solution to the Mg plates and thus reduces its corrosion rate. It is further observed that among the Mg–HA composite films coated Mg plates, the impedance of the composite coated Mg plates having higher amount of HA is more. This suggests that the coating having higher amount of HA provides more impedance to the electrons and ions to reach at surface of Mg, and thus will be more corrosion protective in nature. The observed EIS results are in good correlation with the results obtained using potentiodynamic polarization study. Song *et al.*^[38] have also observed that the electrodeposited hydroxyapatite, using $\text{Ca}(\text{NO}_3)_2$, $\text{NH}_4\text{H}_2\text{PO}_4$, and H_2O_2 , on Mg alloy showed higher value of impedance compared to bare Mg alloy. This indicates that the corrosion protective nature of HA on Mg

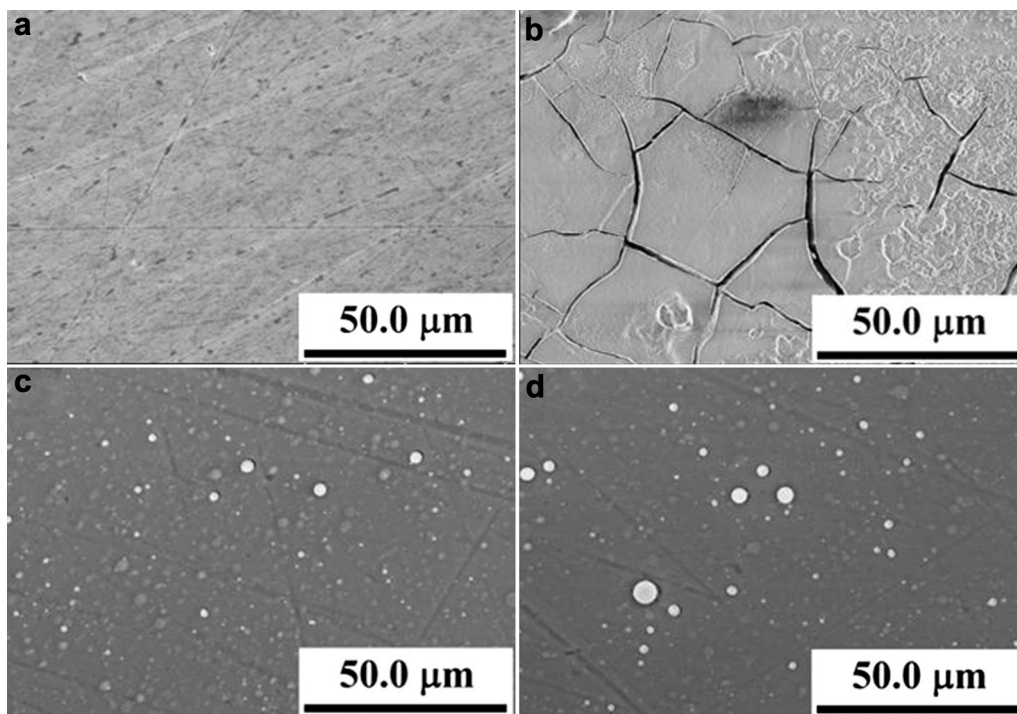


Fig. 9 SEM images of uncoated Mg plate (control) (a) before and (b) after corrosion experiments. SEM images of Mg plate coated with 50Mg–50HA composite film before (c) and after (d) corrosion experiments.

alloy. In order to understand the corrosion process of uncoated Mg plate and Mg plates coated with Mg–HA composite films in greater detail, samples were analyzed under SEM before and after the corrosion study. Selected sample morphologies before and after corrosion testing are shown in Fig. 9. As seen in these figures, the uncoated Mg plate shows considerable corrosion with cracks which can lead to pitting and crevice corrosion thereby accelerating the degradation of Mg plate. However, the Mg plates coated with Mg–HA composite films do not show significant degradation. This suggests that coatings are dense and prevent the transport of electrons and ions from solution to Mg plates. The observed SEM images further supports the results obtained from potentiodynamic polarization and EIS studies.

4. Conclusion

HA–Mg composite thin films were grown on Mg plates by using a multi-target PLD technique. The composite coatings have been found to render several advantageous characteristics to Mg plates. The advantageous characteristics are in terms of controlled corrosion behavior and superior mechanical properties. These characteristics are expected to result in better integration of Mg implants coated with Mg–HA films with surrounding matrix in the living beings.

Acknowledgments

This research was financially supported by the National Science Foundation through Engineering Research Center of Revolutionizing Metallic Biomaterials at NCAT. Authors thank Dr. J. Sankar, Dr. Y. Yun, and Dr. S. Neralla for useful discussion and providing access to their research facilities.

REFERENCES

- [1] J. Wang, D. Li, X. Yu, X. Jing, M. Zhang, Z. Jiang, J. Alloys Compd. 494 (2010) 271–274.
- [2] G. Wu, X. Zeng, W. Ding, X. Guo, S. Yao, Appl. Surf. Sci. 252 (2006) 7422–7429.
- [3] N.T. Kirkland, J. Lespagnol, N. Birbilis, M.P. Staiger, Corros. Sci. 52 (2010) 287–291.
- [4] Y. Xin, T. Hu, P.K. Chu, Acta Biomater. 7 (2011) 1452–1459.
- [5] H. Homberger, S. Virtanen, A.R. Boccaccini, Acta Biomater. 8 (2012) 2442–2455.
- [6] H. Meifeng, L. Lei, W. Yating, T. Zhixin, H. Wenbin, Corros. Sci. 50 (2008) 3267–3273.
- [7] Y. Mizutani, S.J. Kim, R. Ichino, M. Okido, Surf. Coat. Technol. 169–170 (2003) 143–146.
- [8] S. Zhang, F. Cao, L. Chang, J. Zheng, Z. Zhang, J. Zhang, C. Cao, Appl. Surf. Sci. 257 (2011) 9213–9220.
- [9] X. Zhang, Z. Zhao, F. Wu, Y. Wang, J. Wu, J. Mater. Sci. 42 (2007) 8523–8528.
- [10] Y. Al-Abdullat, S. Tsutsumi, N. Nakajima, M. Ohta, H. Kuwahara, K. Ikeuchi, Mater. Trans. 42 (2001) 1777–1780.
- [11] J.L. Arias, M.B. Mayor, J. Pou, Y. Leng, B. León, M.P. Amor, Biomaterials 24 (2003) 3403–3408.
- [12] J.E. Gray, B. Luan, J. Alloys Compd. 336 (2002) 88–113.
- [13] X.B. Chen, N. Birbilis, T.B. Abbott, Corrosion 67 (2011) 035005.
- [14] B.D. Ratner, Biomaterials Science: An Introduction to Materials in Medicine, Elsevier Academic Press, 2004.
- [15] M. Geetha, D. Durgalakshmi, R. Asokamani, Recent Patents Corr. Sci. 2 (2010) 40–45.
- [16] X. Gu, W. Zhou, Y. Zheng, L. Dong, Y. Xi, D. Chai, Mater. Sci. Eng. C 30 (2010) 827–832.
- [17] S. Hiromoto, A. Yamamoto, Electrochim. Acta 54 (2009) 7085–7093.
- [18] F. Witte, F. Feyerabend, P. Maier, J. Fischer, M. Störmer, C. Blawert, W. Dietzel, N. Hort, Biomaterials 28 (2007) 2163–2174.
- [19] T.J. Webster, C. Ergun, R.H. Doremus, R. Bizios, J. Biomed. Mater. Res. 59 (2002) 312–317.
- [20] T.J. Webster, E.A. Massa-Schlueter, J.L. Smith, E.B. Slamovich, Biomaterials 25 (2004) 2111–2121.
- [21] C.M. Serre, M. Papillard, P. Chavassieux, J.C. Voegel, G. Boivin, J. Biomed. Mater. Res. 42 (1998) 626–633.
- [22] X.B. Chen, N. Birbilis, T.B. Abbott, Corros. Sci. 53 (2011) 2263–2268.
- [23] B.D. Hahn, D.S. Park, J.J. Choi, J. Ryu, W.H. Yoon, J.H. Choi, H. E. Kim, S.G. Kim, Surf. Coat. Technol. 205 (2011) 3112–3118.
- [24] W. Mróz, A. Bombalska, S. Burdyńska, M. Jedyński, A. Prokopiuk, B. Budner, A. Ślósarczyk, A. Zima, E. Menaszek, A. Ścisłowska-Czarnecka, J. Mol. Struct. 977 (2010) 145–152.
- [25] R. Eason, Pulsed Laser Deposition of Thin Films: Applications-led Growth of Functional Materials, Wiley-Interscience, Hoboken, N.J., 2007.
- [26] G.P. Dinda, J. Shin, J. Mazumder, Acta Biomater. 5 (2009) 1821–1830.
- [27] Q. Bao, C. Chen, D. Wang, T. Lei, J. Liu, Mater. Sci. Eng. A 429 (2006) 25–29.
- [28] R.E. Honig, RCA Rev. 23 (1962) 567–586.
- [29] S. Neralla, D. Kumar, S. Yarmolenko, J. Sankar, Compos. Part B: Eng. 35 (2004) 157–162.
- [30] V. Nelea, H. Pelletier, P. Mille, D. Muller, Thin Solid Films 453–454 (2004) 208–214.
- [31] V. Nelea, H. Pelletier, D. Müller, N. Broll, P. Mille, C. Ristoscu, I.N. Mihailescu, Appl. Surf. Sci. 186 (2002) 483–489.
- [32] H. Kim, R.P. Camata, S. Chowdhury, Y.K. Vohra, Acta Biomater. 6 (2010) 3234–3241.
- [33] A.N. Chamos, C.A. Charitidis, A. Skarmoutsou, S.G. Pantelakis, Fatigue Fract. Eng. Mater. Struct. 33 (2010) 252–265.
- [34] B. Landkof, Materialwiss. Werkst 34 (2003) 395–399.
- [35] M. Stern, J. Electrochem. Soc. 104 (1957) 559–563.
- [36] C. Wen, S. Guan, L. Peng, C. Ren, X. Wang, Z. Hu, Appl. Surf. Sci. 255 (2009) 6433–6438.
- [37] H.Y. Ma, C. Yang, S.H. Chen, Y.L. Jiao, S.X. Huang, D.G. Li, J.L. Luo, Electrochim. Acta 48 (2003) 4277–4289.
- [38] Y.W. Song, D.Y. Shan, E.H. Han, Mater. Lett. 62 (2008) 3276–3279.